Bias in Intracellular Luminescence Thermometry: The Case of the Green Fluorescent Protein

Paloma Rodríguez-Sevilla,* Graham Spicer, Ana Sagrera, Alejandro P. Adam, Alejo Efeyan, Daniel Jaque,* and Sebastian A. Thompson*

Measurement of intracellular temperature in a fast, accurate, reliable, and remote manner is crucial for the understanding of cellular processes. Nanothermometers based on the green fluorescence protein (GFP) are of special interest because intracellular temperature readouts can be obtained from the analysis of the polarization state of its luminescence. Despite the good results provided by GFP thermometers, the reliability of their intracellular thermal readouts is still a question of debate. Here, light is shed on this issue by introducing cell activity as a relevant bias mechanism that prevents the use of GFP for reliable intranuclear thermal measurements. Experimental evidence that this lack of reliability can affect not only GFP but also other widely used thermometers such as semiconductor nanocrystals is provided. It is discussed how differences observed between calibration curves obtained in presence and absence of cell activity can inform about the presence of bias. The presented results and discussion are aimed to warn the community working in intracellular thermometry and encourage authors to approach the issue in a conscious manner. The performance and reliability of the chosen intracellular thermometers must be judiciously assessed. This is the only way intracellular thermometry can progress and deliver indisputable results.

1. Introduction

Temperature is a fundamental parameter for any living organism. The potential measurement of fast temperature changes at the micro- and nanoscales with high precision would enable the comprehensive study of intracellular thermal processes such as those responsible for thermoregulation, or those linked to changes in metabolism.[1,2] Of special relevance is the measurement of temperature in particular organelles such as the mitochondrion or the nucleus whose natural activity involves adenosine triphosphate (ATP)-consuming reactions that are associated to heat generation.[3–5] In pursuit of the accurate measurement of temperature in biological systems, different thermometric techniques have been developed.[6] Due to its remote character, one of the preferred choices is luminescence thermometry, where the temperature changes are detected through the variations in the thermosensitive fluorescence properties (e.g., intensity, lifetime, polarization) of the fluorescent molecule or particle (thermometer) that is used as sensor.[7–9] In addition, some of these probes can target cellular regions and organelles for localized temperature measurements.[10,11] Examples of luminescent thermometers used in intracellular studies encompass metallic and dielectric particles,[12–14] semiconductor nanomaterials,[15] nanodiamonds,[13]

P. Rodríguez-Sevilla, D. Jaque
Nanomaterials for Bioimaging Group (NanoBIG)
Departamento de Física de Materiales
Universidad Autónoma de Madrid
C/ Francisco Tomás y Valiente 7, 28049 Madrid, Spain
E-mail: paloma.rodriguez@uam.es; daniel.jaque@uam.es
G. Spicer
Wellman Center for Photomedicine
Massachusetts General Hospital
Boston, MA 02114, USA
G. Spicer
Harvard Medical School
Harvard University
Boston, MA 02115, USA

The ORCID identification number(s) for the author(s) of this article can be found under https://doi.org/10.1002/adom.202201664.

A. Sagrera, A. Efeyan
Centro Nacional de Investigaciones Oncológicas (CNIO)
28029 Madrid, Spain
A. P. Adam
Department of Molecular and Cellular Physiology and Department of Ophthalmology
Albany Medical Center
Albany, NY 12208, USA
D. Jaque
Nanomaterials for Bioimaging Group (NanoBIG)
Instituto Ramon y Cajal de Investigación Sanitaria IRYCIS
Ctra Colmenar Km 9-100, 28034 Madrid, Spain
S. A. Thompson
Madrid Institute for Advanced Studies in Nanoscience
(IMDEA Nanociencia)
C/ Faraday 9, 28049 Madrid, Spain
E-mail: sebastian.thompson@imdea.org
S. A. Thompson
Nanobiotechnology Unit Associated to the National Center
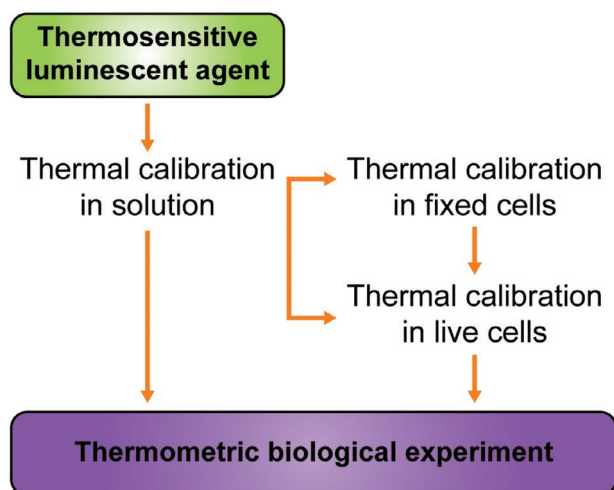for Biotechnology (CNB-CSIC-IMDEA)
28049 Madrid, Spain

**ADVANCED
SCIENCE NEWS**
www.advancedsciencenews.com

**ADVANCED
OPTICAL
MATERIALS**
www.advopticalmat.de

Figure 1. Typical structure of studies on luminescence thermometry where a luminescent thermometer is calibrated and applied to measure temperature in a cellular experiment.

carbon-based nanomaterials,[16] polymers,[17] DNA-based thermometers,[18] and polymer nanoparticles doped with lanthanide complexes,[19] fluorescent dyes and proteins.[20,21]

During the last few years, the use of luminescent thermometers for intracellular thermal sensing has been very intense. This is evidenced in Table S1 (Supporting Information) that includes an extensive list of the different approaches adopted for intracellular thermal sensing. In all the cases, the procedure used for intracellular thermometry follows the same route (see **Figure 1**). First, the emission properties of the luminescent probe (absolute intensity, relative intensity between bands, spectral shift, luminescence lifetime, or polarization) are recorded as a function of temperature to build a calibration curve. From the calibration curve, the authors determine the relative thermal sensitivity of the probe, that is typically considered as the figure of merit.[22] This first calibration is performed with the thermometer dispersed in aqueous media (calibration in solution). In some cases, calibration curves are also measured in live cells to assess the applicability of the thermometer for intracellular thermometry.[10–12,15,18,21,23–43] We found few cases that perform this second calibration in fixed cells[21,34] (see Table S1 in the Supporting Information). Finally, the potential of the intracellular thermometer is validated by a biological experiment aimed to measure intracellular thermal changes produced by, for instance, heat production inside the cell. We have not included in Table S1 (Supporting Information) those studies that, although present a probe for intracellular thermometry, do not actually show any experimental validation inside live cells.

Although the working procedure shown in Figure 1 and adopted in most of the works listed in Table S1 (Supporting Information), is widely accepted in the community, it oversimplifies the complexity of intracellular measurements. For intracellular thermometry, one should consider the change in environmental conditions that the thermometer experiences when transferred from the colloidal dispersion to the interior of the cell. It is known that the intracellular environment is extremely complex and constantly changing. Parameters such as pH, ionic strength, protein concentration, and viscosity are present in an inhomogeneous distribution within the cell. Most importantly, temporal variation in these parameters and other physical properties (e.g., molecular structure, volume) occur when the state of the cell or organelle is perturbed. This is a crucial factor in experiments intended to measure thermal changes generated by an external stimulus that affects the state of the cell (e.g., transcriptional or metabolic activity). Due to these interfering factors, the calibration curve of the thermometer measured in controlled conditions (solution and fixed cells) can be completely different than that obtained in live cells. This is indeed revealed by Table S1 (Supporting Information) in which it is evidenced that in most cases, the thermal sensitivities obtained in living cells differ significantly from those obtained in solution.

The existence of differences between the calibration curves obtained in aqueous solutions and in cells is known by the community and makes it surprising that more than 30% of the studies we reviewed go directly from calibration in solution to their in vitro application (see Table S1 in the Supporting Information). Most studies (72%) take a more thorough approach and experimentally study possible confounding factors (e.g., pH, thermometer concentration, ionic strength, protein concentration, and viscosity) that can interfere with intracellular thermal measurement. We have also found evidence in the literature of changes in thermometric signal and thermal sensitivity of the thermometer when internalized by different cell lines.[17,18,23,26,43] This may indicate the presence of unknown factors that still play an important role in the nanothermometer's signal and have not been deeply studied and discussed by the scientific community.

One of the most popular luminescent thermometers for intracellular measurements is green fluorescence protein (GFP). In our case, the thermal readout is based on the temperature-induced variations in the fluorescence polarization anisotropy (FPA), as it has been reported for a variety of systems.[20,44–46] GFP-based luminescent thermometers are of special relevance because they can be self-produced by cells minimizing cytotoxicity and stress. As schematically represented in **Figure 2**a, GFP is naturally located inside the nucleus (Figure 2b) attached to the histone H2B (H2B–GFP) allowing for contactless reading of nuclear temperature that might be related to changes in cellular activity associated with gene expression. We selected H2B since this protein is one of the histone proteins involved in the structure of chromatin. Genomic DNA is wrapped, protected, and packed in the nucleus in the form of chromatin (Figure 2a), mainly consisting of histones (purple regions) and DNA (in blue) that form tight DNA–protein interactions.[47] Chromatin condensation state plays a unique role regulating transcription. It has been extensively reported that the chemical modifications of histones induce chromatin relaxation (i.e., transition from close to open chromatin, Figure 2a). This relaxation facilitates the transcription machinery to bind DNA and begin transcription at those loci. Relaxation and transcription require profound enzyme-based, ATP-consuming remodeling of the DNA–histone interactions. Such intranuclear processes might produce profound changes in the intranuclear temperature that, in principle, could be measured using an optical thermometric technique with subdegree and nanoscale resolution. Acetylation of histones, in our case H2B, controls the level of gene expression and thus cellular activity. This cell activity control is performed
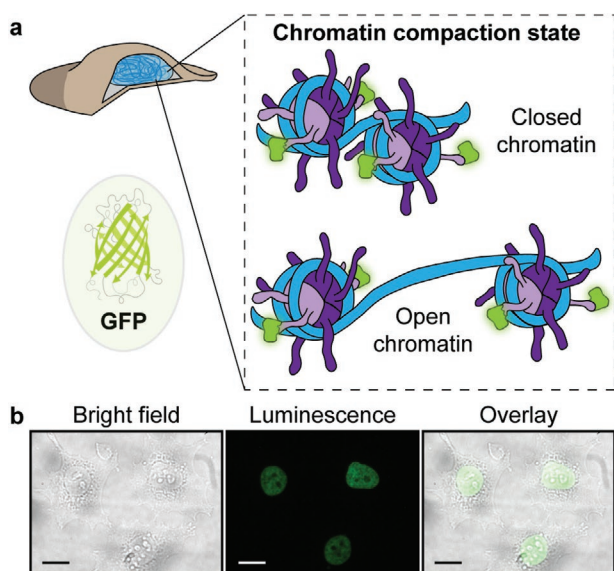
Figure 2. Chromatin and H2B–GFP. a) Schematic representation of a cell transfected with H2B–GFP. Cellular activity changes produce a transition from closed to open chromatin for the DNA to be accessed and replicated. We used a green fluorescence protein (GFP, green region) fused to histone H2B (light purple region) to measure thermal changes produced when histone (purple regions) modification induces chromatin compaction variations. b) Bright field, fluorescent (false color), and overlay images of three H2B–GFP transfected cells. Scale bars are 20 µm.

by the transition from closed to open chromatin for the DNA to be accessed and replicated (Figure 2). Detection of nuclear temperature by measuring the FPA of H2B–GFP could constitute the basis of advance diagnosis and controlled treatment of diseases such as cancer or metabolic disorders,[48,49] and could assist for a deeper understanding of cellular senescence, quiescence, and aging in cell culture and live organism.[50,51] Despite of its interest, the reliability of GFP–H2B as an intranuclear thermometer still remains to be established.

In this work, we have critically analyzed the reliability of intranuclear thermometry in living cells by using H2B–GFP as FPA-based thermometer. Comparison between calibration curves obtained in solution, fixed, and live cells has been performed to evaluate how the thermal responses of H2B–GFP thermometers are affected by environmental conditions. We include different experiments to reveal the presence of relevant bias during thermal monitoring inside the nucleus using H2B–GFP as FPA-based thermometer. We also provide evidence that similar bias could also affect intracellular measurements performed by using other well-known luminescent nanothermometers such as CdSe quantum dots (QDs). The discussion, conclusions, and proposed approaches we present in this paper are aimed to boost the progress of intracellular thermometry, rather than discourage researchers from pursuing this goal.

2. Working Principle and Calibration of H2B–GFP for Intranuclear Thermometry

Thermal reading through FPA is based on the temperature dependence of the polarization state of the radiation generated by fluorescent molecules. These emit light that is polarized along a particular direction. As the molecule rotates due to Brownian motion, the detected light will be an average of all emitted polarization directions. At variance with other approaches based on pure intensity measurements, the ratiometric character of FPA-based temperature readings makes them independent on the local concentration of fluorescent molecules and less affected by fluctuations in the excitation intensity. The FPA value characterizes the difference in polarization (i.e., depolarization degree or anisotropy) between the linearly polarized excitation and the light emitted by the molecule. It is a ratio calculated using the emission at two orthogonal polarization states (see the Experimental Section), one being parallel to the excitation.[52,53] The link between the experimentally measured FPA value and the mobility of the molecule is given by the Perrin equation

$$\text{FPA} = \frac{r_0}{1 + \dfrac{\tau_f}{\Theta_r}} \tag{1}$$

where r_0 is a constant delimiting the anisotropy value to a theoretical maximum, τ_f (s) is the fluorescence lifetime of the fluorophore, and Θ_r (s) its rotational correlation time.[52] While τ_f is defined by the photophysical characteristics of the fluorophore, Θ_r depends on its hydrodynamic properties as

$$\Theta_r = C \frac{\eta}{k_B T} \tag{2}$$

where k_B is the Boltzmann constant; and C (m³) depends on the shape of the molecule,[54,55] being the hydrodynamic volume for a sphere or $L^3/Ln(L/D)$ for a cylinder (where L and D are the length and diameter, respectively).[56] The rotational motion of the fluorescent molecule depends on the temperature, T (K), and the solvent viscosity, η (Pa s), which is also thermally dependent. This, together with the fact that the fluorescent lifetime might also vary with temperature, implies that any thermal change will affect the FPA value, converting the fluorescent macromolecule into a thermometer. It is important to note that viscosity does not only depend on temperature, but also on many other parameters such as medium density or local structure (physicochemical properties of medium). This precludes the existence of an unequivocal relation between the FPA value and temperature inside the cells. Relevant bias in intracellular measurements could occur when the changes in FPA induced by the physicochemical changes taking place in live cells are comparable to those induced by temperature variations. The magnitude of those "activity-related FPA fluctuations" has never been explored and, thus, the occurrence of relevant bias when using GFP for intracellular sensing in live cells remains an open question.

GFP expressed intracellularly in live cells has been used as a FPA-based thermometer to estimate the cytoplasmic temperature changes produced by an external heat source.[20] In our case, GFP's performance inside the nucleus (particularly attached to the histone H2B) is expected to be different due to the changes in the environment of the fluorescent molecule. To assess this, we first tested H2B–GFP in a controlled
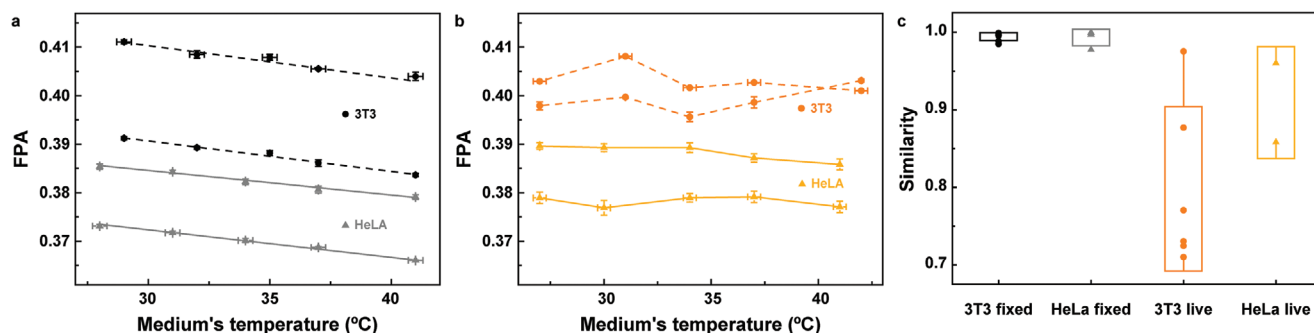
**ADVANCED
SCIENCE NEWS**

www.advancedsciencenews.com

**ADVANCED
OPTICAL
MATERIALS**

www.advopticalmat.de

Figure 3. Thermal calibrations. Evolution of the FPA value as a function of the medium's temperature for a) 4 fixed H2B–GFP transfected cells and b) 4 live H2B–GFP transfected cells. Error bars are the standard deviation of 5 consecutive measurements. Lines in panel (a) correspond to the best linear fit. c) Similarity between the thermal calibrations in fixed and live cells. In all panels, data include results for 3T3 (dots) and HeLa (triangles) nuclei.

environment with similar properties to the nucleus of a live cell. The closest model one can find is the nucleus of a fixed cell. We fixed human epithelioid cervix carcinoma (HeLa) cells and NIH 3T3 mouse embryonic fibroblast cells expressing H2B–GFP and changed their temperature to obtain the calibration curve (see the Experimental Section). Our experimental systems allowed us to take two images of the nuclear intensity for two orthogonal polarizations (see the Experimental Section). Using these images, we constructed the FPA map of the nucleus for each temperature to obtain the FPA distribution per pixel (see Figure S1 in the Supporting Information). The assigned FPA value for each temperature is the central value of the distribution.

In **Figure 3**a, we show representative results obtained for 4 fixed HeLa and 3T3 nuclei. The measured FPA value differs between cell lines and individual cells of the same type. However, the same thermal response is observed in all the cases: the FPA value decreases when the temperature increases, in agreement with previous studies.[42,44–46,57] We calculated, for each nucleus, the slope of the evolution of FPA with temperature $\left(\frac{dFPA}{dT}\right)$. Although the FPA value differs between cells, the mean FPA versus T slope is independent of the cell line (see the Supporting Information), with a value of $-0.5 \pm 0.1 \times 10^{-3}$ °C^{-1}. The statistical error obtained for the mean values are around the 20%, which agrees with the expected uncertainty due to cellular variability. The monotonic linear trend followed by the FPA value in all the cases suggests that H2B–GFP can provide reliable intranuclear temperature measurements in fixed cells. However, is it worth noting that, since the FPA value is not the same for each cell, our technique can only allow us to measure temperature changes rather than absolute temperature values.

We next tested the reliability of H2B–GFP as nuclear FPA-based thermometer in live cells, i.e., during normal cell activity. Representative results of the FPA value measured for 4 live cells (including HeLa and 3T3 cells) subjected to different mediums' temperatures are shown in Figure 3b. The decreasing linear trend observed for fixed cells is lost and, for most of the cells, the FPA value remains almost constant in the temperature range (note that Figure 3a,b has the same y-axis limits). This could be explained without resorting to bias by assuming that the intracellular temperature remains constant at 27 °C independently of the medium temperature. This would imply that

intracellular thermoregulation is capable of stablishing a cell–medium temperature difference as large as 13 °C. Thermoregulation does exist in live cells and could lead to differences between medium and intracellular temperatures but not of such magnitude. If the presence of cell thermoregulation was responsible of the differences between the calibration curves in fixed and live cells, such differences should be observed always, independently on the luminescent nanothermometer. But this is not the case. For instance, Na Wu et al. found the same calibration curves in fixed and live cells when working with nonbiased lanthanide-doped nanothermometers.[58]

In Figure 3a,b, the FPA errors (vertical scale) have been calculated as the standard variation of 5 measurements. The calculated errors in the determination of FPA are not evident in these figures because they are much smaller than the absolute value of FPA. On average, the error in determining the FPA value for each temperature is ±0.001 in fixed cells and ±0.002 in live cells. These errors are more than two orders of magnitude smaller than the absolute values of FPA (≈0.4). When working with live cells, the experimental errors were larger than when working with fixed cells. This, together with the differences between calibration curves obtained in fixed and live cells, suggests that cell activity (and the fluctuations that it causes on the intranuclear structure) impacts on the value of FPA so that it avoids an unequivocal correlation between FPA values and temperature in live cells.

To analyze the decorrelation between temperature and FPA in live cells, we have calculated the similarity between the mean sensitivity of fixed and live cells

$$\text{Similarity} = 1 - \left| \frac{\sum_j \left(\text{FPA}_j^{\text{exp}} - \text{FPA}_j^{\text{fix}} \right)^2}{\sigma} \right| \qquad (3)$$

where $\text{FPA}_j^{\text{exp}}$ are the experimental FPA values for each temperature j, $\text{FPA}_j^{\text{fix}}$ is the FPA value calculated for the fixed cells at the temperature j (see Table S2 in the Supporting Information), and σ denotes the standard deviation of the experimental FPA values ($\text{FPA}_j^{\text{exp}}$). The calculated similarities for all fixed and live nuclei are included in Figure 3c. When the experimental values follow a similar trend to the mean curve observed for fixed cells, the similarity approaches unity, as occurs for fixed

**ADVANCED
SCIENCE NEWS**

www.advancedsciencenews.com

**ADVANCED
OPTICAL
MATERIALS**

www.advopticalmat.de

cells (i.e., the trends for fixed cells are similar to their mean). When the experimental trend diverges, the similarity decreases, as is the case of most of the live cells. The dispersion in the similarity values also highlights the decorrelation between the FPA value and temperature for live cells (see the Supporting Information for the complete analysis).

Results included in Figure 3 show that the anisotropy signal of the H2B–GFP molecules in live cells is strongly influenced by nuclear changes not correlated with temperature (i.e., bias does exist). Equations (1) and (2) state that the viscosity of the surrounding medium (the nuclear viscosity in the case of H2B–GFP) modulates the FPA value. As mentioned above, transcriptional activity results in changes in the chromatin conformation (compaction/relaxation state, see Figure 2a). Moreover, changes in the external temperature impact several cellular processes, such as gene expression that requires chromatin decompaction.[59–62] Such activity-related variations could induce changes in the local nuclear viscosity that have an impact on the mobility of H2B–GFP molecules, thus, on their polarized emission properties. These changes are not expected in fixed cells, where the compaction state of the chromatin is constant as cell activity is suppressed. In this case, H2B–GFP molecules are only subjected to the changes in temperature. In addition, it has been reported that the lifetime of GFP changes with the temperature and viscosity of the environment.[27,63,64] Thus, activity-related variation in the nucleus structure impacts on the FPA value of H2B–GFP and precludes any direct correlation between temperature and FPA value. In order words, in the presence of cell activity, a reliable intranuclear calibration curve cannot be obtained. To give further proof of the existence of this bias, we have designed two experiments where we monitored the FPA of H2B–GFP while the chromatin condensation state is controllably altered. These experiments are based on an external biological (serum starvation–replenishment experiments) or chemical (osmotic shock) perturbation that produces a change in the nucleus. As we show in the following sections, these two experiments are proof of the care that one must take when measuring temperature during a profound cellular change.

3. Biological Perturbation: Serum Starvation–Replenishment Experiments

In cultured cells, growth factors present in fetal bovine serum (FBS) are required for growth and proliferation. FBS is generally supplemented up to 10% of the culture medium volume. Withdrawal of FBS from the medium and readdition are typically used to analyze acute cellular responses via signal transduction cascades that activate cellular programs to elicit cell growth and proliferation.[65] One outcome of these intracellular signaling cascades is the execution of transcriptional programs that require significant rearrangements of chromatin compaction. Such epigenetic changes in DNA and histones exert topological changes that result in an "open conformation" of the chromatin for the genes to be expressed (Figure 2a), allowing transcription factor binding and RNA polymerase activity. Cells deprived of FBS enter an arrested state of low metabolism (low activity). When serum is readded to the culture medium, the cells transduce signals within seconds and increase their

metabolism in a time lapse of few tens of minutes entering again the proliferative state and continue the cell cycle (normal activity).[66–69]

The transition from arrested to proliferative state is expected to have an impact on the nuclear viscosity and temperature (i.e., thermal rise when cellular activity increases) and, thus, on the FPA of H2B–GFP molecules. In the absence of any bias, the arrested-to-proliferative state should be accompanied by an increment in the intranuclear temperature and, therefore, to a reduction in the FPA of H2B–GFP. To corroborate this, we monitored the nuclear FPA value of live and fixed transfected HeLa cells during different serum starvation–replenishment experiments at a constant controlled temperature (see the Experimental Section). Paraformaldehyde-fixed cells served as a control for the potential existence of optical artifacts due to the addition of serum (see the Supporting Information). As an additional control, we used live cells kept at room temperature, which present a lower metabolism,[59,67,70] thus are expected to have a much slower response to serum than cells at 37 °C.

In **Figure 4**a, we show the results of the serum starvation–replenishment experiments we performed with three cell populations: live cells at 37 °C (orange data), live cells at room temperature (21 °C, dark cyan data), and fixed cells at 37 °C (black data). We tracked the medium's temperature during the experiments (see top graph in Figure 4a) that remains almost constant with fluctuations below 1 °C. We monitored the cells in the arrested state for at least 20 min before adding serum (time = 0 min, green arrow in Figure 4a), and then we followed their response for 40 min more during the proliferative state. We calculated the FPA change as the FPA value at each time point minus the average FPA value in the arrested state (i.e., before adding serum).

As shown in Figure 4a, each cell population showed a different response. We present the mean trend for the live cells at room temperature (dark cyan data) and fixed cells (black data) because the variability was much lower than in the case of the live cells kept at 37 °C (orange data), for which we show a single cell as a representative example. The individual responses of every cell studied can be found in the Supporting Information. Despite the variability, the behavior of the live cells kept at 37 °C was similar within the population but distinct to the other cell populations (see Figure S3 in the Supporting Information). Results obtained for fixed cells (black data in Figure 4a) show that the FPA value remains almost constant within statistical error. This proves that, in absence of cellular activity, the chromatin state is not modified, consequently, the viscosity does not vary. In addition, using a thermal slope of $-0.5 \pm 0.1 \times 10^{-3}$ °C^{-1}, the mean thermal variation calculated from the standard deviation of the FPA change after serum addition is around 2 °C, that sets the temperature resolution in the serum starvation–replenishment experiments.

On the other hand, live cells at 37 °C (orange data in Figure 4a) show an increase in the FPA value that reaches a maximum (point A) and then decays to a value that is close to that of the arrested state (point B). In the case of live cells kept at a lower temperature, the average trend shows that the maximum takes longer to be reached (around 30 min, point A), and the FPA value does not decrease to reach the arrested level in the time frame studied. If these changes in FPA were correlated
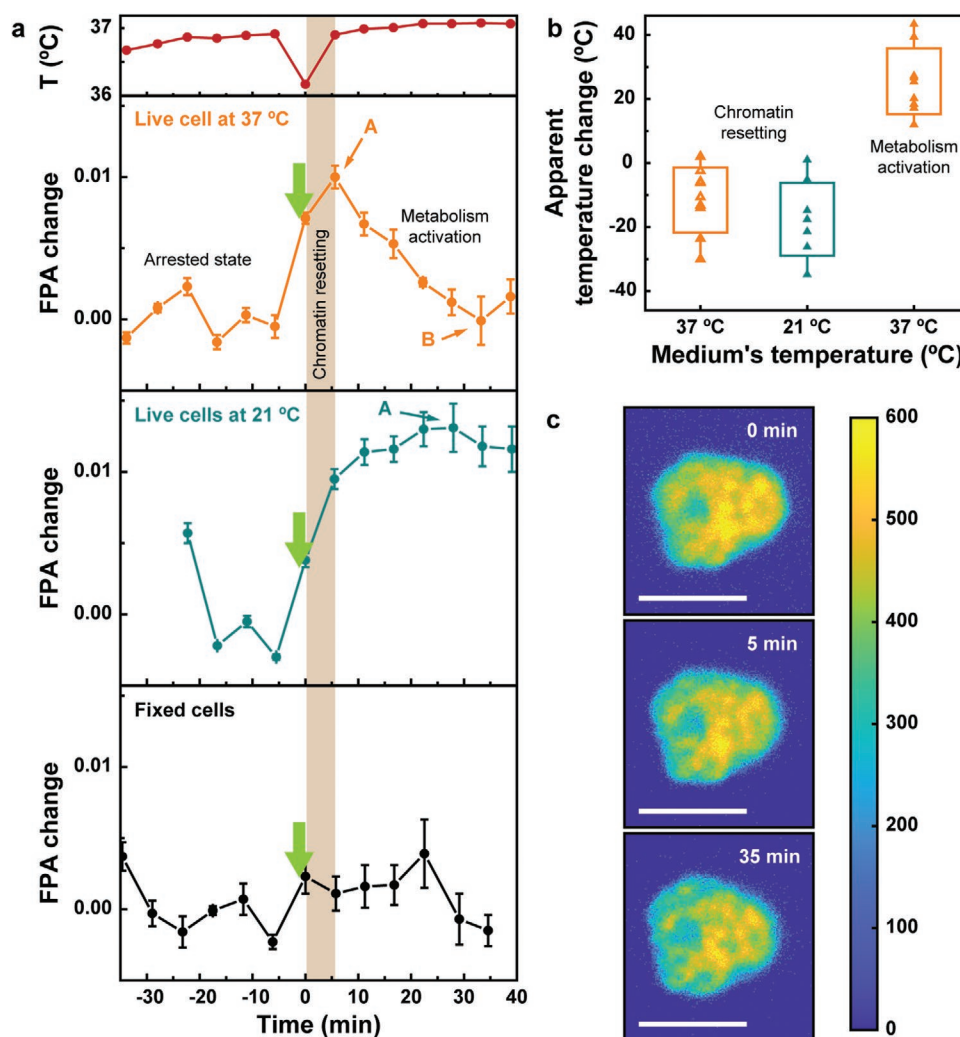
Figure 4. Effect of the biological stimulus. a) Evolution of the FPA value in respect to the mean value in the arrested state (time < 0), i.e., we subtracted the mean FPA value before adding serum to each data point. The addition of serum is indicated with a green arrow. Data in orange represent a single live cell kept at 37 °C. Dark cyan and black data represent the mean trend obtained from 4 live cells kept at 21 °C and 3 fixed cells kept at 37 °C, respectively. Data in red are the medium's temperature associated to the live cell data at 37 °C. Error bars are the standard deviation. b) Temperature changes estimated from the FPA variation between $t = 0$ and point A (chromatin resetting) and the variation between points A and B (metabolism activation). c) Intensity images of the live cell nucleus shown in panel (a) at three time points (before serum and at points A and B). Scale bars are 10 µm.

to variations in the nuclear temperature, and assuming a FPA versus temperature slope of -0.5×10^{-3} °C^{-1}, experimental data would indicate an intranuclear thermal change in the range -30 to 2 °C and -34 to 1 °C for cells kept at 37 and 21 °C, respectively (see Figure 4b, chromatin resetting data). For the cells kept at 37 °C, we can also calculate an apparent temperature change associated to the activation of the cellular metabolism (decrease in the FPA change between points A and B). In this case, the estimated intranuclear apparent temperate increases between 12 and 43 °C (see Figure 4b). For live cells kept at low temperature, the FPA signal remains almost constant after the maximum is reached, thus we do not calculate a temperate change. We associate this to a lower response of the cells that do not increase their metabolism in the time frame of our experiment.[71]

The "apparent" thermal changes (either increase or decrease) calculated from the analysis of the FPA that are shown in

Figure 4b have been obtained by considering that FPA only depends on temperature and results unreliable. The magnitude of these calculated temperature variations (tens of degrees) is very unlikely to take place in a biological system. Moreover, the initial increase in the FPA signal (between $t = 0$ and point A) implies a decrease in the temperature. For this time window after the addition of serum, we expect the temperature to remain constant or at least present a much smaller increase than during the cell activation (between points A and B). These results evidence that FPA-based GFP thermometers are inadequate for intranuclear temperature sensing because they are biased (the FPA output depends on other factors than solely the temperature).

Data included in Figure 4b reveal the lack of an unequivocal relation between the FPA of H2B–GFP and intranuclear temperature. The question now is to determine what is exactly causing the changes in FPA observed during the serum

starvation–replenishment experiments. As discussed above, H2B–GFP is subjected to environmental changes derived from variations in the chromatin compaction state that potentially affect both the fluorescent lifetime of the molecule and the viscosity that drags its movement. To confirm the presence of intranuclear structural changes during the serum starvation–replenishment experiments, we analyzed the intensity images generated by H2B–GFP since the variation of the intensity of intranuclear fluorescent markers (e.g., Hoechst, GFP) is known to be a common tool to detect changes in the compaction state of the chromatin. For the case of H2B–GFP, it is well accepted that it can show the DNA packing density in different regions of the nucleus, appearing as brighter the regions of higher compaction.[47] In Figure 4c, we show three intensity images of the nucleus of the live cell at 37 °C (Figure 4a, orange data). Right after the addition of serum (0 min), the intensity map has larger regions of high intensity in the center of the nucleus, showing that the chromatin is mostly in a high compaction state (heterochromatin) associated to a lower gene expression. This is in good agreement with the fact that cells deprived of FBS remain in an arrested state of low metabolism. After the chromatin resetting period (5 min), the average intensity decreases leading to smaller regions of high intensity. 35 min after the addition of serum, the intensity distribution is different to when the stimulus was produced (compare 0 and 35 min). After the metabolism activation period, larger regions of low intensity associated to higher levels of gene expression (euchromatin) have appeared. We did not observe these intensity changes in live cells kept at 21 °C, where the intensity distribution remained almost the same with no apparent changes between regions of high and low intensity (see Figure S9 in the Supporting Information). Thus, Figure 4c reveals the presence of relevant changes in the intranuclear compaction states that explains the changes in the FPA during a serum starvation–replenishment experiment. In conclusion, results included in Figure 4 evidence the presence of an interfering factor (i.e., chromatin compaction changes) that affects the FPA value and hampers the measurement of temperature from the simple analysis of the FPA of H2B–GFP. Finally, we should note that this argument also explains the different time evolutions of FPA prior the serum addition observed for the three cases analyzed in Figure 4a, i.e., in their "basal" state. In the case of live cells, the FPA in the basal state shows relevant fluctuations with time that are not observed in the case of fixed cells. This can be again explained by considering that FPA signal is strongly linked to the intranuclear compaction state and that remains unperturbed in fixed cells but fluctuates due to cellular activity in live cells.

4. Chemical Perturbation: Osmotic Shock

Hyperosmotic shock is widely reported in the literature as a chemical-based stimulus that induces instantaneously cell dehydration, cell volume decreases, and, thus, molecular crowding, due to efflux of water from the cell.[72] Concerning the nucleus structure, it has been shown that hyperosmotic shock induces first a fast increase in the chromatin condensation state (physical response), followed by a slow response when the cell tries to regain the osmotic equilibrium (biological response).[72–74] We do not expect the first process to induce any thermal variation inside the nucleus, so this first response to osmotic shock constitutes a good scenario to study how the luminescence of GFP is altered by changes in the intranuclear structure in the absence of temperature variations. In other words, if the FPA signal is unequivocally related to temperature, it should remain constant during the cellular response to osmotic shock, i.e., while the cell changes its transcription state to accommodate to the homeostasis stress.

To monitor the variation of FPA signal in HeLa cells subjected to a hyperosmotic shock, we designed a similar experiment to the one we used for the biological stimulus (see the Experimental Section). In this case, we added NaCl to the culture medium of cells kept at a constant temperature of 37 °C. As we expected the chemical stimulus to produce a faster cell response, we took consecutive images of the cells after the addition at a higher rate than in the biological perturbation experiment. As before, we calculated the FPA change as the difference between the FPA value at each instant and the average FPA value before NaCl addition. Results shown in **Figure 5**a correspond to the mean trend of 6 live HeLa cells kept at around 37 °C (see the Supporting Information for the individual response of each cell). Experimental data reveal how the FPA value drastically decreases after addition of NaCl (marked with a green arrow). When looking in detail to the first moments after the addition of NaCl (Figure 5b), it is clear how the FPA signal reaches its minimum value in less than 1 min. After this, it starts to recover. This recovery it is not complete and the FPA value does not recover its "basal" value even after times as long as 40 min (Figure 5a).

If the FPA change would be attributed solely to a thermal variation and using the same FPA versus T slope for H2B–GFP as in Section 3, the apparent temperature change estimated from the decrease in the FPA value (change between the point A in Figure 5a and the value before NaCl addition) is in the range 31–82 °C (see Figure 5b). As for the case of the biological perturbation, these temperature variations are not compatible to cellular thermodynamics.[75] Furthermore, as explained before, the intranuclear temperature is expected to remain unaltered during the response to the osmotic shock. Thus, this reflects the lack of reliability of the H2B–GFP as FPA-based intranuclear nanothermometer in presence of structural changes. This lack of reliability can be, again, explained in terms of the changes in chromatin compaction that takes place in response to the osmotic shock. Hyperosmotic stress produces an initial fast physical response when the nucleus "dries out" leading to chromatin condensation that generates a nonhomogeneous distribution with large regions of free chromatin (interchromatin domain).[72,73] This effect can be seen in the total intensity maps of Figure 5d. Before addition of NaCl, the nucleus shows a distribution of high intensity and low intensity regions comparable to the total intensity map of a nucleus with normal nuclear activity (see Figure 4c, 35 min). After the hyperosmotic shock (Figure 5d, 0.3 s), the intensity map clearly shows the condensation of the chromatin in particular regions leading to large interchromatin domains. After this initial fast response, cells present a long-term adaptation to the hyperosmotic stress that involves the increase in the expression of certain genes that
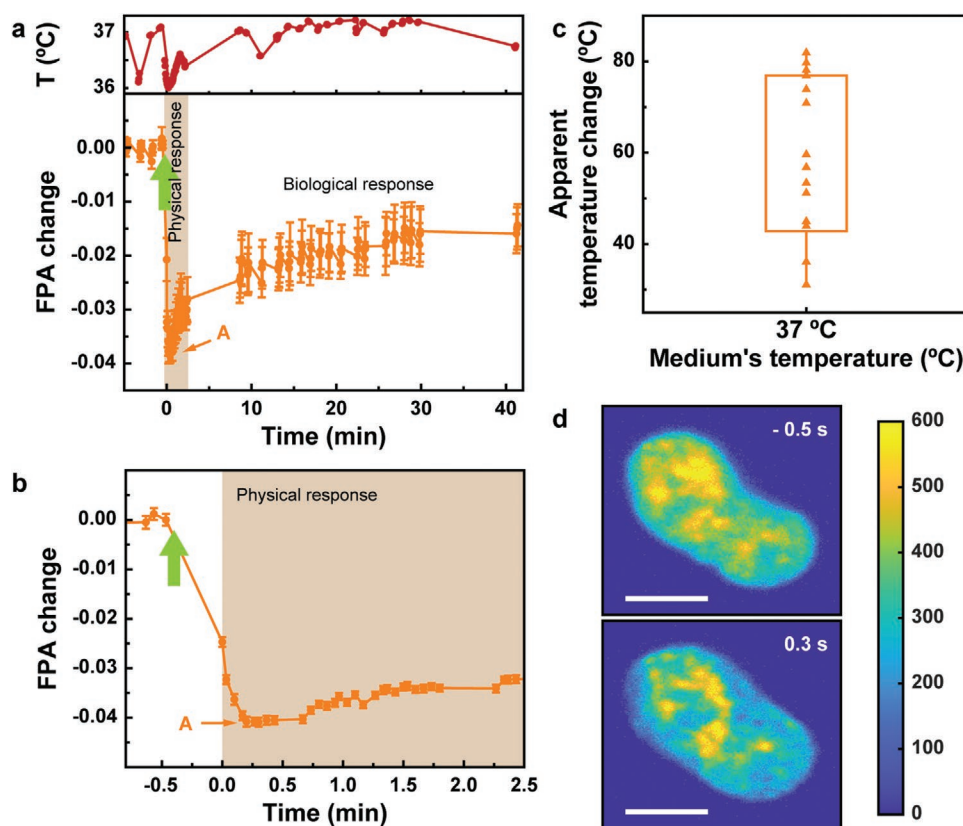
Figure 5. Effect of the chemical stimulus. a) Evolution of the FPA value in respect to the mean value before addition of NaCl (instant marked with a green arrow). Data correspond to the mean trend of 6 HeLa cells kept at around 37 °C (see red data). Error bars are the standard deviation. b) FPA change of a single cell during the first minutes after addition of NaCl. Error bars correspond to the error from the Gaussian fit. c) Temperature changes estimated from the maximum FPA variation (point A in panels (a) and (b)) after the addition of NaCl. d) Intensity images of the nucleus in (b) for two time points (right before NaCl addition and at point A). Scale bar is 10 μm.

allow the cells to regain the homeostasis.[73] The FPA signal shows this response (biological response in Figure 5a) that takes place in a time scale similar to the metabolic activation shown in Figure 4a.

In conclusion, results included in Figure 5 again evidence that the changes in chromatin compaction affect the FPA value and make it impossible to obtain a reliable thermal reading.

5. Predicting Bias in Intracellular Luminescence Thermometry from Calibration Curves

Previous sections revealed how, for the case of H2B–GFP FPA-based thermometers, reliable intracellular thermal measurements are not possible because of the existence of bias. This was not only proved by the anomalous thermal readouts obtained in experiments performed on live cells (where structural changes occur even in the absence of temperature variations), but it was already evidenced from the calibration experiments: calibration curves obtained in solution (or fixed cells) and live cells (in absence and presence of cell activity) differ significantly. In fact, the reproducibility of the calibration curves obtained in different conditions is the first difference between "ideal" and "biased" thermometers (see schematic representation in **Figure 6**). The signal output of an "ideal"

thermometer only depends on its temperature so that environmental changes caused by cell activity do not affect its calibration curve (Figure 6a). In this case, the calibration curves obtained in live cells and in solution or fixed cells are identical. Also, when working with live cells, there is an unequivocal relation between the signal provided by the luminescent nanothermometer and the intracellular temperature. On the other hand, a "biased thermometer" is characterized by showing calibration curves that depend on the environmental conditions and/or on the presence of cell activity (see Figure 6b). In a "biased thermometer," the calibration curves obtained in fixed and live cells do not overlap because temperature is not the only parameter determining the signal provided by the thermometer. In this case, the cell activity can produce changes in the signal output of the thermometer that can be erroneously attributed to changes in intracellular temperature (Figure 6b). According to this, the existences of differences in the calibration curves obtained in absence and presence of cell activity or in different environmental conditions are a clear warning of lack of reliability in intracellular thermal measurements.

To extend these conclusions to other nanothermometers, we performed osmotic shock experiments utilizing polymeric encapsulated CdS/ZnS semiconductor QDs as nanothermometers in HeLa cells. The preliminary results that support our conclusions are illustrated in Figure S11 (Supporting Information).
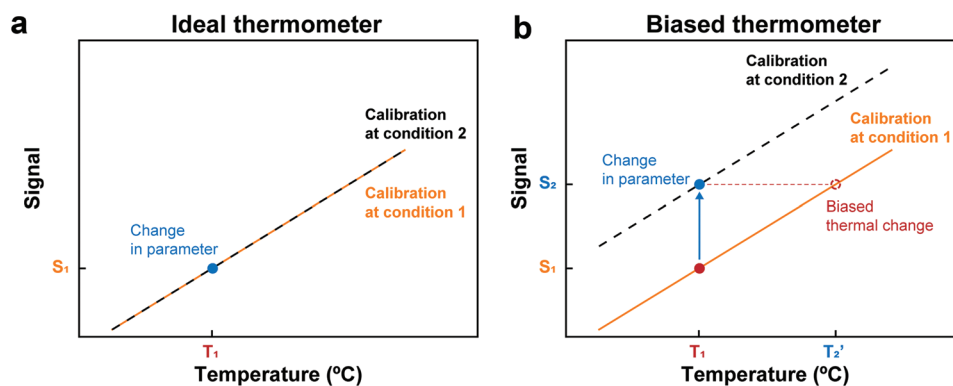
Figure 6. Mislabeling of temperature. Comparison between a) an ideal thermometer and b) a biased thermometer. In the ideal case, both the thermal response and the absolute value of the signal remain constant under a change of an external parameter (i.e., calibrations at conditions 1 and 2 are exactly the same). Thus, only thermal changes produce a change in the signal that can be directly related to the temperature variation. In the biased case, the thermal sensitivity is independent of the external factor (i.e., calibrations at conditions 1 and 2 have the same slope), but the absolute signal varies. Thus, a change in this external parameter produces a variation of the signal that is associated to a nonexisting thermal change that gives an erroneous temperature (T_2').

These results reveal that the lack of reliability in intracellular thermal sensing experiments is not restricted to the FPA-based nanothermometers, but could be affecting other widely used systems.

6. Conclusions

In this paper, we have investigated the performance of H2B–GFP FPA-based intranuclear fluorescence thermometer and discuss the main interfering factors that hamper its use for reliable measurement of intracellular temperature. We prove how changes in the thermometer (FPA) signal provided by H2B–GFP can be easily misunderstood if one does not consider the occurrence of a biased thermal reading. We demonstrate that changes in the chromatin compaction state via cell activity modulation or via chemical perturbations induce changes in the FPA signal of H2B–GFP thermometers that can be erroneous interpreted as temperature changes. This work also anticipates the scientific community that the presence of such bias is not restricted to H2B–GFP thermometers but could affect other nanothermometers with great potential for intracellular measurements. As an example, we have also performed experiments in live cells incubated with QD-intensity-based thermometers. It is also found that in this system, the change in the compositional properties of intracellular medium can induce changes in the QD signal that can be erroneously interpreted as thermal variations.

The experimental evidence here found together with the extensive literature review performed make us think that bias is present in a relevant fraction of intracellular thermometry studies and might have been the origin of controversial results. We also believe that these pitfalls and complications can be the reason why only 44% of the studies we analyzed focus on the measurement of temperature within specific organelles. Thus, we state that bias in intracellular thermometry could be avoided by the development of inert thermal probes, researchers should redirect their efforts not only to give colloidal stability to the samples through their coatings, but also to isolate them from

the environment. These coatings can act as a barrier that isolates the thermometer from surrounding molecules, preventing its signal from being affected by other parameters than temperature. We state that this is one of the paths that should be followed toward reliable intracellular thermal thermometry.

With this article, we would like to show that the measurement of intracellular temperature is not a trivial task, especially under biological or chemical stimulus and at organelle level. Far from presenting a pessimistic view of the future of intracellular thermometry, we would like to encourage the community to pursue this goal in a conscious manner. Finally, we strongly believe that, although interferences might prevent confident interpretation of intracellular thermal measurements, one can take advantage of them. Since the information included in the variation of the thermometer signal may be the combination of temperature and other variables, it could also carry important new information that currently might remain mislabeled as "temperature" but could be the basis of novel intracellular sensing techniques.

7. Experimental Section

Reagents: Dulbecco's modified Eagle medium (DMEM)–Glutamax (31966 057), penicillin–streptomycin (15070-063), and DMEM without phenol red (21063-029) were purchased from GIBCO. Fetal bovine serum (SV30160.3) from HyClone was heat inactivated at 56 °C for 30 min before use. X-treme Gene 9 transfection reagent (6365787001, Roche), 35 mm culture dishes with 20 mm treated glass bottom surface (734 2904, VWR). Plasmid pγH2B–GFP was a kind gift of Dr. Quintana Laboratory at CNIOM.

Cell Culture and Preparation: Human epithelioid cervix carcinoma (HeLa) cells and NIH 3T3 mouse embryonic fibroblast cells were maintained in DMEM–Glutamax medium (31966 057, Gibco), supplemented with 10% fetal bovine serum (SV30160.3, Hyclone) and penicillin–streptomycin (15070-063, Gibco), at 37 °C, 5% CO_2 atmosphere. For the experiments, 35 000 cells were plated on 35 mm culture dishes with 20 mm treated glass bottom surface (734 2904, VWR), in a final volume of 2 mL of growing medium. 24 h after seeding, the cells were transfected with plasmid pγH2B–GFP, using X-treme Gene 9 transfection reagent (6365787001, Roche) at a ratio XG9:DNA (3:1), according to the manufacturer's instructions. 24 h

after transfection, the medium was replaced and, 24 h before the measurements (72 h after transfection), the complete medium was replaced by medium with antibiotic and without serum. The day of the experiment, the medium was changed for DMEM without phenol red and without serum, with a 20 μM final concentration of 4-(2-hydroxyethyl)-1-piperazineethanesulfonic acid (HEPES) to keep optimal pH during the experiments. For fixation, the cells were washed 3 times with phosphate-buffered saline (PBS) and then fixed using 4% paraformaldehyde/PBS solution for 30 min at 37 °C. After washing, the cells were kept in PBS. QDs (Qtracker 525 Cell Labeling Kit, Q25041MP) were obtained from Thermofisher. First, 10 nM labeling solution was prepared by premixing 1 μL each of Qtracker Component A and Component B in a 1.5 mL microcentrifuge tube. After 5 min incubation at room temperature, 0.2 mL of fresh complete growth medium was added to the tube and vortexed for 30 s. This 0.2 mL was added to the culture dishes and the cells were incubated in normal conditions for 60 min. After this, cells were washed with complete growth medium. Consecutive washing procedures were performed to ensure that QDs were inside cells.

Optical Setup: The experiments were performed in two different experimental systems that had the same layout based on commercial inverted microscopes (Leica DMi8 S widefield epifluorescence microscope with incubation system for time-lapse studies – system A – and Eclipse Ti2-U, Nikon – system B). this was done to show that interferences in intranuclear thermometry were independent on the experimental system. The measured FPA value was expected to be different for each setup due to the differences in the optical elements. In both experimental systems, images were taken with a scientific complementary metal oxide semiconductor (sCMOS) camera (Orca-Flash4.0, Hamamatsu) coupled to a beam divider (W-viewer Gemini, Hamamatsu). The beam divider allowed to obtain two separate images of the same field of view (FOV) on the same camera chip. The sample was excited with linearly polarized light. In each of the two paths created by the beam divider, a linear polarizer was placed, oriented either parallel or perpendicularly to the polarization of the excitation light. In this way, two images of the emission of the fluorophores with orthogonal polarization were obtained. To excite the H2B–GFP and QDs, the light coming from a 488 nm laser was focused in epi mode with a 100×, 1.47 numerical aperture (NA) HC PL APO OIL objective lens (Leica) – system A – or the light coming from a light emitting diode (LED) lamp (pE-300light-series, CoolLED) onto the sample using a 50×, 0.35 NA objective lens (SLMPLN, Olympus) – system B. An irradiation power of less than 1 mW and reduced irradiation time (few seconds) and number of repetitions (3–5) were used to minimize photobleaching of the fluorophores and phototoxicity. A fluorescence filter cube was used for the GFP emission (Ex. 481–495 nm, DC495, Em. 500–550 nm) – system A – or the filter cube 19002-AT-GFP/FITC Longpass (Chroma) – system B – to filter both excitation and emission lights.

Analysis of the Images: The FPA value was obtained from the recorded frames using homemade scripts developed with Matlab software. Each measured frame was composed by two images of the same FOV. The images corresponded to two orthogonal polarizations of the fluorophore emission, one parallel ($I_\parallel$) and other perpendicular ($I_\perp$) to the excitation. The two images were matched and the FPA value, $(I_\parallel - I_\perp)/(I_\parallel + 2I_\perp)$, was calculated for every pixel to construct the FPA maps. The different nuclei in the FOV were selected to calculate their FPA value. For the whole nuclear area, the FPA value distributions were obtained (number of pixels vs FPA value, see the Supporting Information) and then fitted to a Gaussian to obtain the central value. The images were not subjected to any modification when calculating the FPA value, just the intrinsic, constant intensity background of the camera produced by electronic noise was subtracted prior analysis.

Thermometry: For the evaluation of the response of H2B–GFP to temperature, the temperature of the medium was controlled using a stage top incubator (Okolab) – system A – or a heated plate (Linkam) and monitored with a thermocouple (Pico Technology) – system B. The medium temperature was changed in steps and let to stabilize for

at least 10 min before taking 5 consecutive frames. The sensitivity of H2B–GFP response to temperature corresponded to the slope of the linear fit of the FPA value evolution with temperature.

Serum Starvation–Replenishment Experiments: These experiments were performed in system B. Cells were maintained in medium without serum overnight. Before the experiment, the medium was replaced by 1 mL of medium with no serum and no phenol red with 20 μM of HEPES. 3 sets of frames were taken every 5 min prior adding 100 μL of serum (10% final concentration). The first image of the proliferating state was taken few tens of seconds after the addition of serum. Then, taking 3 sets of frames every 5 min was continued for at least 30 min more. The cells were kept at a constant temperature.

Osmotic Shock Experiments: These experiments were performed in system B. Before the experiment, the medium was replaced by 1 mL of medium without phenol red, and with 20 μM of HEPES. 3 sets of frames were taken every 5 min prior adding NaCl solution to the medium to reach 350 mOsm L^{-1} osmolarity. Few seconds after the addition, the first frame was taken of a series of consecutive frames during ≈2 min. Then, sets of three consecutive images were taken between variable periods to track the evolution of the signal during ≈40 min.

Supporting Information

Supporting Information is available from the Wiley Online Library or from the author.

Acknowledgements

Conflict of Interest

The authors declare no conflict of interest.

Author Contributions

P.R.-S. performed and analyzed the cellular experiments. G.S. contributed to the analysis of the data. A.S., A.A., and A.E. provided the transfected cells and the biological background to perform the experiments. D.J. actively participated in the development of the study and scientific discussions. S.A.T. conceived the project, participated in the cellular experiments and preparation of the cells. P.R.-S., D.J., and S.A.T. wrote the paper with contribution of all authors.

Data Availability Statement

The data that support the findings of this study are available from the corresponding author upon reasonable request.

[1] K. Skok, M. Duh, A. Stožer, A. Markota, M. Gosak, *WIREs Mech. Dis.* **2021**, *13*, e1513.

[2] K. Okabe, S. Uchiyama, *Commun. Biol.* **2021**, *4*, 1377.

[3] M. R. Depaoli, F. Karsten, C. T. Madreiter-Sokolowski, C. Klec, B. Gottschalk, H. Bischof, E. Eroglu, M. Waldeck-Weiermair, T. Simmen, W. F. Graier, R. Malli, *Cell Rep.* **2018**, *25*, 501.

[4] T. Enomoto, S.-I. Tanuma, M.-A. Yamada, *J. Biochem.* **1981**, *89*, 801.

[5] M. Sawadogo, R. G. Roeder, *J. Biol. Chem.* **1984**, *259*, 5321.

[6] K. M. McCabe, M. Hernandez, *Pediatr. Res.* **2010**, *67*, 469.

[7] J. Zhou, B. del Rosal, D. Jaque, S. Uchiyama, D. Jin, *Nat. Methods* **2020**, *17*, 967.

[8] M. Quintanilla, L. M. Liz-Marzán, *Nano Today* **2018**, *19*, 126.

[9] C. W. Chung, G. S. Kaminski Schierle, *ChemBioChem* **2021**, *22*, 1546.

[10] S. Kiyonaka, T. Kajimoto, R. Sakaguchi, D. Shinmi, M. Omatsu-Kanbe, H. Matsuura, H. Imamura, T. Yoshizaki, I. Hamachi, T. Morii, Y. Mori, *Nat. Methods* **2013**, *10*, 1232.

[11] M. Nakano, Y. Arai, I. Kotera, K. Okabe, Y. Kamei, T. Nagai, *PLoS One* **2017**, *12*, e0172344.

[12] Y. Wang, S. Liang, M. Mei, Q. Zhao, G. She, W. Shi, L. Mu, *Anal. Chem.* **2021**, *93*, 15072.

[13] Y. Wu, M. N. A. Alam, P. Balasubramanian, A. Ermakova, S. Fischer, H. Barth, M. Wagner, M. Raabe, F. Jelezko, T. Weil, *Nano Lett.* **2021**, *21*, 3780.

[14] X. Di, D. Wang, J. Zhou, L. Zhang, M. H. Stenzel, Q. P. Su, D. Jin, *Nano Lett.* **2021**, *21*, 1651.

[15] H. Liu, Y. Fan, J. Wang, Z. Song, H. Shi, R. Han, Y. Sha, Y. Jiang, *Sci. Rep.* **2015**, *5*, 14879.

[16] L. Shi, D. Chang, G. Zhang, C. Zhang, Y. Zhang, C. Dong, L. Chu, S. Shuang, *RSC Adv.* **2019**, *9*, 41361.

[17] K. Okabe, N. Inada, C. Gota, Y. Harada, T. Funatsu, S. Uchiyama, *Nat. Commun.* **2012**, *3*, 705.

[18] G. Ke, C. Wang, Y. Ge, N. Zheng, Z. Zhu, C. J. Yang, *J. Am. Chem. Soc.* **2012**, *134*, 18908.

[19] K. M. Kuznetsov, V. A. Baigildin, A. I. Solomatina, E. E. Galenko, A. F. Khlebnikov, V. V. Sokolov, S. P. Tunik, J. R. Shakirova, *Molecules* **2022**, *27*, 8813.

[20] J. S. Donner, S. A. Thompson, M. P. Kreuzer, G. Baffou, R. Quidant, *Nano Lett.* **2012**, *12*, 2107.

[21] S. Arai, S. C. Lee, D. Zhai, M. Suzuki, Y. T. Chang, *Sci. Rep.* **2014**, *4*, 6701.

[22] C. D. S. Brites, P. P. Lima, N. J. O. Silva, A. Millán, V. S. Amaral, F. Palacio, L. D. Carlos, *Nanoscale* **2012**, *4*, 4799.

[23] T. Hayashi, N. Fukuda, S. Uchiyama, N. Inada, *PLoS One* **2015**, *10*, e0117677.

[24] S. Uchiyama, T. Tsuji, K. Ikado, A. Yoshida, K. Kawamoto, T. Hayashi, N. Inada, *Analyst* **2015**, *140*, 4498.

[25] Y. Takei, S. Arai, A. Murata, M. Takabayashi, K. Oyama, S. Ishiwata, S. Takeoka, M. Suzuki, *ACS Nano* **2014**, *8*, 198.

[26] D. Chrétien, P. Bénit, C. Leroy, R. El-Khoury, S. Park, J. Y. Lee, Y.-T. Chang, G. Lenaers, P. Rustin, M. Rak, *Chemosensors* **2020**, *8*, 124.

[27] P. L. Silva, O. A. Savchuk, J. Gallo, L. García-Hevia, M. Bañobre-López, J. B. Nieder, *Nanoscale* **2020**, *12*, 21647.

[28] O. A. Savchuk, O. F. Silvestre, R. M. R. Adão, J. B. Nieder, *Sci. Rep.* **2019**, *9*, 7535.

[29] T. Zhao, K. Asawa, T. Masuda, A. Honda, K. Kushiro, H. Cabral, M. Takai, *J. Colloid Interface Sci.* **2021**, *601*, 825.

[30] M. Homma, Y. Takei, A. Murata, T. Inoue, S. Takeoka, *Chem. Commun.* **2015**, *51*, 6194.

[31] D. Chrétien, P. Bénit, H.-H. Ha, S. Keipert, R. El-Khoury, Y.-T. Chang, M. Jastroch, H. T. Jacobs, P. Rustin, M. Rak, *PLoS Biol.* **2018**, *16*, e2003992.

[32] J. Qiao, C. Chen, D. Shangguan, X. Mu, S. Wang, L. Jiang, L. Qi, *Anal. Chem.* **2018**, *90*, 12553.

[33] N. Xie, J. Huang, X. Yang, X. He, J. Liu, J. Huang, H. Fang, K. Wang, *Anal. Chem.* **2017**, *89*, 12115.

[34] Z. Huang, N. Li, X. Zhang, C. Wang, Y. Xiao, *Anal. Chem.* **2018**, *90*, 13953.

[35] L. Shang, F. Stockmar, N. Azadfar, G. U. Nienhaus, *Angew. Chem., Int. Ed.* **2013**, *52*, 11154.

[36] F. Dong, T. Zheng, R. Zhu, S. Wang, Y. Tian, *J. Mater. Chem. B* **2016**, *4*, 7681.

[37] J. Qiao, C. Chen, L. Qi, M. Liu, P. Dong, Q. Jiang, X. Yang, X. Mu, L. Mao, *J. Mater. Chem. B* **2014**, *2*, 7544.

[38] J. Qiao, Y. H. Hwang, C. F. Chen, L. Qi, P. Dong, X. Y. Mu, D. P. Kim, *Anal. Chem.* **2015**, *87*, 10535.

[39] J. Qiao, Y. H. Hwang, D. P. Kim, L. Qi, *Anal. Chem.* **2020**, *92*, 8579.

[40] Y. Wu, J. Liu, J. Ma, Y. Liu, Y. Wang, D. Wu, *ACS Appl. Mater. Interfaces* **2016**, *8*, 14396.

[41] C. Gota, K. Okabe, T. Funatsu, Y. Harada, S. Uchiyama, *J. Am. Chem. Soc.* **2009**, *131*, 2766.

[42] J. S. Donner, S. A. Thompson, C. Alonso-Ortega, J. Morales, L. G. Rico, S. I. C. O. Santos, R. Quidant, *ACS Nano* **2013**, *7*, 8666.

[43] S. Arai, M. Suzuki, S. J. Park, J. S. Yoo, L. Wang, N. Y. Kang, H. H. Ha, Y. T. Chang, *Chem. Commun.* **2015**, *51*, 8044.

[44] S. A. Thompson, I. A. Martinez, P. H. González, A. Adam, D. Jaque, J. B. Nieder, R. De Rica, *ACS Photonics* **2018**, *5*, 2676.

[45] G. Baffou, M. P. Kreuzer, F. Kulzer, R. Quidant, *Opt. Express* **2009**, *17*, 3291.

[46] G. Spicer, S. Gutierrez-Erlandsson, R. Matesanz, H. Bernard, A. P. Adam, A. Efeyan, S. Thompson, *J. Biophotonics* **2021**, *14*, 202000341.

[47] T. Kanda, K. F. Sullivan, G. M. Wahl, *Curr. Biol.* **1998**, *8*, 377.

[48] C. Sotiriou, L. Pusztai, *N. Engl. J. Med.* **2009**, *360*, 790.

[49] I. Barroso, M. I. McCarthy, *Cell* **2019**, *177*, 146.

[50] T. Anwar, B. Sen, S. Aggarwal, R. Nath, N. Pathak, A. Katoch, M. Aiyaz, N. Trehanpati, G. Khosla, S. Ramakrishna, *J. Cell. Physiol.* **2018**, *233*, 3695.

[51] C. K. Lee, R. G. Klopp, R. Weindruch, T. A. Prolla, *Science* **1999**, *285*, 1390.

[52] D. M. Jameson, J. A. Ross, *Chem. Rev.* **2010**, *110*, 2685.

[53] J. R. Lakowicz, in *Principles of Fluorescence Spectroscopy*, Springer, Boston, MA **2006**, pp. 353–382.

[54] J. L. Dote, D. Kivelson, R. N. Schwartz, *J. Phys. Chem.* **2002**, *85*, 2169.

[55] L. Zhang, M. L. Greenfield, *J. Chem. Phys.* **2010**, *132*, 184502.

[56] M. Doi, *J. Phys. (France)* **1975**, *36*, 607.

[57] G. Spicer, A. Efeyan, A. P. Adam, S. A. Thompson, *J. Biophotonics* **2019**, *12*, 201900044.

[58] F. L. Na Wu, Y. Sun, M. Kong, X. Lin, C. Cao, Z. Li, W. Feng, *Small* **2022**, *18*, 2107963.

[59] P. Gong, C.-S. Li, R. Hua, H. Zhao, Z.-R. Tang, X. Mei, M.-Y. Zhang, J. Cui, *PLoS One* **2012**, *7*, e35313.

[60] T. R. Kießling, R. Stange, J. A. Käs, A. W. Fritsch, *New J. Phys.* **2013**, *15*, 045026.

[61] H. Tomoda, Y. Kishimoto, Y. C. Lee, *J. Biol. Chem.* **1989**, *264*, 15445.

[62] J. R. Subjeck, J. J. Sciandra, C. F. Chao, R. J. Johnson, *Br. J. Cancer, Suppl.* **1982**, *5*, 127.

**ADVANCED
SCIENCE NEWS**

www.advancedsciencenews.com

**ADVANCED
OPTICAL
MATERIALS**

www.advopticalmat.de

[63] A. D. Kummer, C. Kompa, H. Niwa, T. Hirano, S. Kojima, M. E. Michel-Beyerle, *J. Phys. Chem. B* **2002**, *106*, 7554.

[64] K. Suhling, D. M. Davis, D. Phillips, *J. Fluoresc.* **2002**, *12*, 91.

[65] T. J. Langan, K. R. Rodgers, R. C. Chou, *Methods Mol. Biol.* **2016**, *1524*, 97.

[66] Y. Wang, S. Maharana, M. D. Wang, G. V. Shivashankar, *Sci Rep.* **2014**, *26*, 4477.

[67] L. Hunt, D. L. Hacker, F. Grosjean, M. De Jesus, L. Uebersax, M. Jordan, F. M. Wurm, *Biotechnol. Bioeng.* **2005**, *89*, 157.

[68] D. Chen, M. Dundr, C. Wang, A. Leung, A. Lamond, T. Misteli, S. Huang, *J. Cell Biol.* **2005**, *168*, 41.

[69] H. Albiez, M. Cremer, C. Tiberi, L. Vecchio, L. Schermelleh, S. Dittrich, K. Küpper, B. Joffe, T. Thormeyer, J. von Hase, S. Yang, K. Rohr, H. Leonhardt, I. Solovei, C. Cremer, S. Fakan, T. Cremer, *Chromosome Res.* **2006**, *14*, 707.

[70] A. Clarke, K. P. P. Fraser, *Funct. Ecol.* **2004**, *18*, 243.

[71] A. Moore, J. Mercer, G. Dutina, C. J. Donahue, K. D. Bauer, J. P. Mather, T. Etcheverry, T. Ryll, *Cytotechnology* **1997**, *23*, 47.

[72] J. D. Finan, F. Guilak, *J. Cell. Biochem.* **2010**, *109*, 460.

[73] J. D. Finan, H. A. Leddy, F. Guilak, *Biochem. Biophys. Res. Commun.* **2011**, *408*, 230.

[74] J. Irianto, J. Swift, R. P. Martins, G. D. McPhail, M. M. Knight, D. E. Discher, D. A. Lee, *Biophys. J.* **2013**, *104*, 759.

[75] N. Lane, *PLoS Biol.* **2018**, *16*, e2005113.